Journal of the Indian Institute of Science
A Multidisciplinary Reviews Journal
ISSN: 0970-4140 Coden-JIISAD

REVIEWS

Developments in Single and Multi-photon Fluorescence Microscopy for High Resolution Imaging

Partha Pratim Mondal, Shilpa Dilipkumar, Kavya M., Raju Regmi and Subhajit B. Purnapatra*

Abstract | Fluorescence imaging has revolutionized the field of Biology and improved our understanding of biological phenomena with super-resolution capabilities. This has become the basic tool for unveiling the biological complex processes in a variety of fundamental studies. In this respect, single and multiphoton fluorescence microscopy have overcome many limitations. While epifluorescence and confocal fluorescence microscopy are being routinely used for diagnostics and study of biomolecules, new developments during the last decade has led to many exciting imaging techniques such as, super-resolution microscopy (STED, STORM, PALM and structured illumination), depth imaging microscopy, multi-focal microscopy and light-sheet microscopy. These techniques have advanced the reach of fluorescence microscopy in many fields ranging from nano-optics to bioimaging. In this brief review article, we will review some of the popular, recent and widely used single and multi-photon fluorescence microscopy techniques.

Fluorescence microscopy has its root in 1845, when Sir John F. W. Herschel reported the first observation of fluorescence in Quinine solution.[1] Thereafter, Sir G. G. Stokes in 1852 discovered that the energy of the emission is always less than that of excitation in a Quinine solution. Quinine was excited with a light of 400 nm and the fluorescence was observed at a shifted wavelength of 450 nm.[2] This is due to the rapid decay to the lowest vibrational level $v = 0$ when excited to highest vibrational level of first excited electronic state S_1. This is termed as Stoke's shift in fluorescence microscopy. Extensive studies and conceptulization of the fluorescence process was due to A. Jablonski in 1935.[3] After these initial findings, the field progressed at a steady pace. Another milestone came when Maria G. Mayer proposed the existence of two-photon transitions using the theory of quantum mechanics which later on led to the development of two-photon microscopy.[4] Half a century before, Abbe theoretically established that the resolution of optical imaging system cannot be infinite but limited by diffraction of light, which is now called as Abbe's diffraction limit.[5,6]

Over the last few decades, the field of fluorescence microscopy and imaging has seen an enormous advancement. This has brought a kind of revolution in Biology and Medicine. To start with, confocal laser scanning fluorescence microscopy was developed and conceptulized by a number of research groups.[7–10] This was then further developed and as a result many variants such as, spinning disc confocal microscopy became available.[11] This was then followed by two-photon excitation[12] that brought in the concept of truely point-by-point scanning. The reason behind this is the small molecular cross-section for two-photon excitation that requires very high photon density which is available only at the focus. Therefore, any fluorescence emission due to two-photon excitation occurs predominantly at the focus. This eliminates the use of pinhole. Then came a series of techniques for super-resolution microscopy. In 1992, 4*pi*-microscopy showed an improved axial resolution by a factor of 4–5 times.[13,14] STED microscopy uses the concept of stimulated depletion of excited electronic state to improve the lateral resolution.[15,16] Structured illumination microscopy uses patterned

Department of Instrumentation and Applied Physics, Indian Institute of Science, Bangalore 560012, Karnataka, India.
**partha@iap.iisc.ernet.in*

illumination followed by measuring the fringes in the Moire pattern to enable super-resolution.[17] This was then followed by localization microscopy which has many variants: PALM,[18] STORM,[19] fPALM[20] and GSDIM.[21] All these techniques are primarily based on single molecule localization followed by marking, to develop the whole structure after many single molecule events have been recorded. These techniques require thousands of frames of single molecule events to reconstruct a single super-resolution image. The disadvantage has been the sacrifice of temporal resolution. A better way to incorporate high temporal resolution is to increase single-molecule events per frame and to engage fast-computing engines for the reconstruction process. Parallely, techniques were developed for fast 3D scanning for minimizing photobleaching and improving signal-to-noise ratio. The stand-out technique called SPIM has been initially proposed by Voie et al.,[22] and further developed by Stelzer et al.[23] This technique employs light-sheet rather than point-illumination along with an orthogonal detection system that helps in reducing both the data exposure and acquisition time. Another simpler way to improve temporal resolution is by dividing the fluorescence signal using a beam-splitter and diverting them to multiple detection arms. Essentially, while one of the detector (CMOS) is in reading mode, the other detector can be in acquisition mode and vice-versa. Moreover, this can be extended to an array of detectors after splitting the beam multiple times.

The future development focuses on extending these techniques towards super-resolution imaging and finding techniques for in-vivo depth imaging. There has been some progress in this direction.[24–26] In this review, we will focus on some of the popular single and multi-photon fluorescence microscopy techniques. We will also briefly go through the current super-resolution imaging techniques. Very recently, depth-imaging has become an important issue but still in the early developmental stage.[24–26]

1 Single Photon Fluorescence Microscopy

As the name suggests, this refers to a class of fluorescence microscopy technique that is based on single-photon excitation (1*PE*) process. In 1*PE* process, a single photon of appropriate energy is absorbed by the molecule for transition to the excited state. If the same transition to the excited singlet state is effected by more than one photon, this is termed as multiphoton excitation process. We show these excitation processes using Jablonski energy diagram in Fig. 1. The molecule is excited by an incoming photon of appropriate energy and gets excited to the higher energy states (excited singlets, S_n; $n > 0$). This can also be achieved by n number of photons of lower energy. The excited molecule then undergoes Stoke-shift before returning to ground state S_0, thereby emitting fluorescent light. In section 2 we brief several imaging techniques based on multiphoton excitation process.

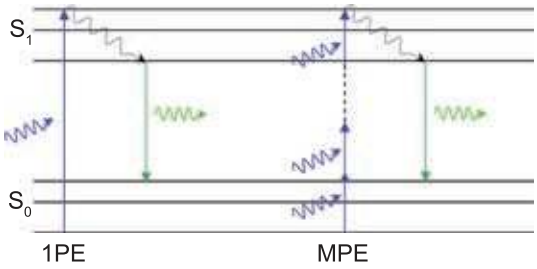

Figure 1: Jabslonski energy diagram for 1PE and MPE processes.

1.1 *Epifluorescence microscopy*

To start with, the simplest form of fluorescence imaging technique is termed as Epifluorescence microscopy. In this technique, the specimen is illuminated throughout and the emitted fluorescence is collected by the detector (CCD/CMOS). Briefly, the illumination light is passed through the emission filter and then focussed by the objective lens on the sample. The emitted fluorescence is then collected by the same lens and directed towards the dichroic mirror. Then, the fluorescent light is made to pass through an appropriate emission filter to remove the scattered and background light. The filtered light is subsequently collected by the collimating lens which is then focused to the detector. Depending upon the position of emission and excitation system, the method can be either trans-illumination (detection and excitation on the either sides of the sample) or epi-illumination (through the objective lens, as shown in Fig. 2). Widefield microscopy is the simplest technique with extensive applications in different domains of science and engineering.

An imaging system is ultimately determined by its point spread function. Following the explicit computable expression of electric field by Wolf and Richards,[78,79] the electric field in particular can be determined at and near the focus of a single aplanatic lens based imaging system. The component of an electric field near the focus of an objective lens for a linearly polarized light illumination is given by[79]

$$\begin{cases} E_x = -iC(I_0 + I_2 \cos 2\phi) \\ E_y = -iCI_2 \sin 2\phi \\ E_z = -2CI_2 \cos \phi \end{cases} \quad (1)$$

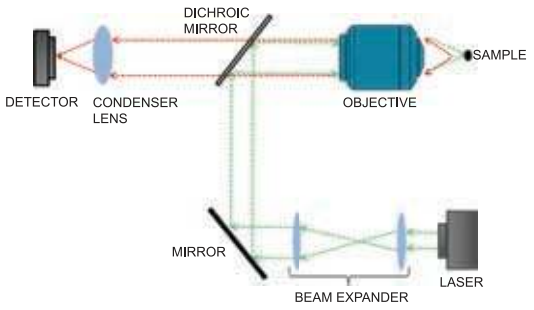

Figure 2: Schematic diagram of Widefield microscopy (epi-illumination).

where the diffraction integrals (with aperture angle α) are defined as

$$\begin{cases} I_0(u,v) = \int_0^{\alpha} \cos^{1/2}\theta' \sin\theta'(1+\cos\theta') \\ \qquad \times J_0\left(\frac{v\sin\theta'}{\sin\alpha}\right) e^{iu\cos\theta'/\sin^2\alpha} d\theta' \\ I_1(u,v) = \int_0^{\alpha} \cos^{1/2}\theta' \sin^2\theta' \\ \qquad \times J_1\left(\frac{v\sin\theta'}{\sin\alpha}\right) e^{iu\cos\theta'/\sin^2\alpha} d\theta' \\ I_2(u,v) = \int_0^{\alpha} \cos^{1/2}\theta' \sin\theta'(1-\cos\theta') \\ \qquad \times J_2\left(\frac{v\sin\theta'}{\sin\alpha}\right) e^{iu\cos\theta'/\sin^2\alpha} d\theta' \end{cases} \quad (2)$$

where, J_0, J_1, J_2 are the Bessel functions of the first kind. The longitudinal and transverse coordinates of a point $P(x, y, z)$ in the region of focus are, $u = kz \sin^2 \alpha$, $v = k(x^2 + y^2)^{1/2} \sin \alpha$ respectively, k being the wave-number.

The excitation PSF for epifluorescence microscopy is

$$\begin{aligned} h_{ill} &= I(u,v,\phi,\lambda_{ill}) = |E_x^{ill}|^2 + |E_y^{ill}|^2 + |E_z^{ill}|^2 \\ &= C_1\left[|I_{0,\lambda_{ill}}|^2 + 2|I_{1,\lambda_{ill}}|^2 + |I_{2,\lambda_{ill}}|^2\right] \end{aligned} \quad (3)$$

where, the components of the electric field are as described above and C_1 is a constant.

The detection PSF for Widefield imaging system is similar to that of illumination PSF except that the emitted wavelength is Stoke-shifted towards higher wavelength. As a result, the detection PSF is essentially a scaled version of illumination PSF. Mathematically, the emission PSF is given by

$$\begin{aligned} h_{det} &= I(u,v,\phi,\lambda_{det}) \\ &= |I_{0,\lambda_{det}}|^2 + 2|I_{1,\lambda_{det}}|^2 + |I_{2,\lambda_{det}}|^2 \end{aligned} \quad (4)$$

The system PSF is given by

$$h_{sys} = h_{exc} \times h_{det} \quad (5)$$

In addition, to enable high temporal resolution along with the spatial resolution, one can employ an array of CMOS cameras multiplexed in time. The emitted fluorescence light can be split and fed to these cameras. During the OFF-state (read-out mode) of the first camera, the second camera can be in acquisition mode (ON-state) and vice-versa. This is schematically shown in Fig. 4A. The system was used to track coated E.Coli cells in a solution for which the results are shown in Fig. 4B. This technique compliments most of the existing fluorescence imaging system.

1.2 *Confocal laser scanning fluorescence microscopy*

Visualization of nanometer sized structures contribute to better understanding of properties and behavior of specimen of interest. In conventional widefield microscopes, the entire sample is illuminated with a light source and the emitted fluorescence is collected. Along with the signal captured from the focal plane, out-of-focus fluorescence is also detected, thus blurring the in-focus details. This greatly reduces the quality and resolution of the acquired images. In addition to the out-of-focus light, scattering also contribute to image degradation. These limitations were overcome by using a optical scanning microscope.[29] In 1957, a postdoctoral fellow from Harvard University, Marvin Minsky[7] examined the idea of using a microscope that used a stage-scanning confocal optical system. A confocal microscope employs a pinhole infront of the detector to eliminate out-of-focus signal, thereby allowing only the light from the focal plane to reach the detector. The aperture stops a large proportion of light from passing through to the detector, so it is essential that only bright sources of light be used.[30] These difficulties were overcome by the advent of laser illumination techniques for scanning the specimen, as introduced by Brakenhoff et al.[28] For a specific setting of the microscope, only a single point on the specimen is acquired at a time. This makes confocal microscopy a serial image acquisition system rather than parallel.[31] Mechanical scanning of the specimen requires a long time to scan the entire specimen. This limitation was largely addressed by two research teams in UK[32] and Sweden[33] by using beam steering methods to scan the specimen. In the confocal configuration, the fluorescence produced by a 3D specimen very close to the focal plane is detected and the axial

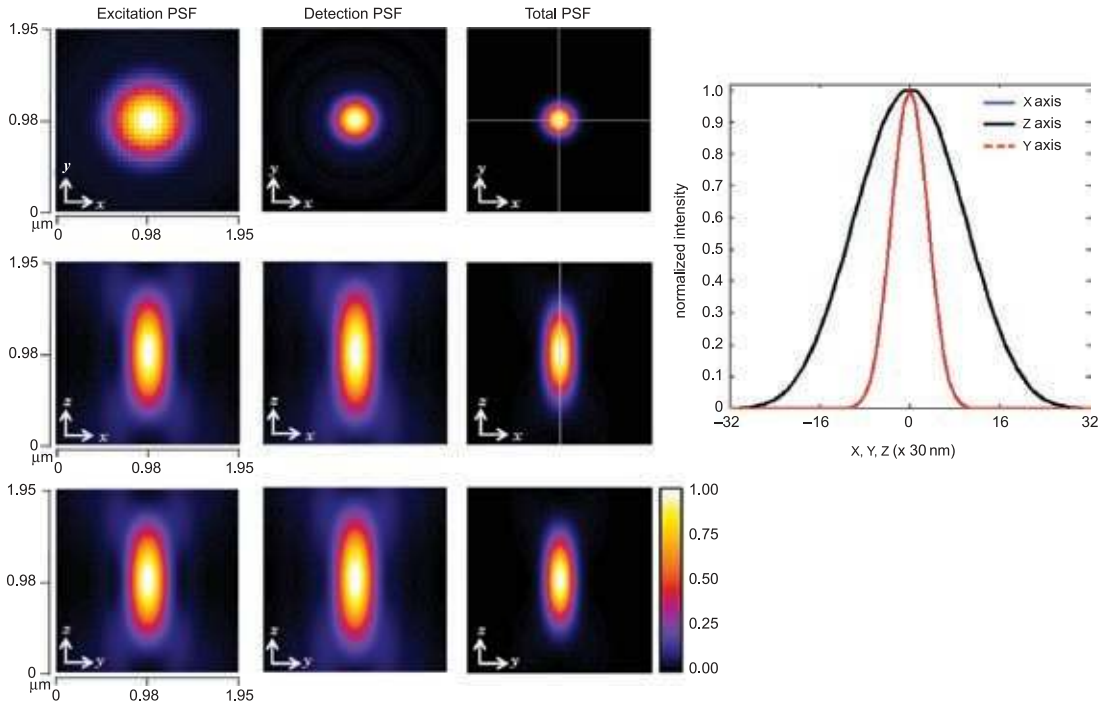

Figure 3: XY, XZ and YZ planes of excitation, detection and system PSF of single-photon excitation epifluorescence microscopy. Alongside, line plots are also shown.

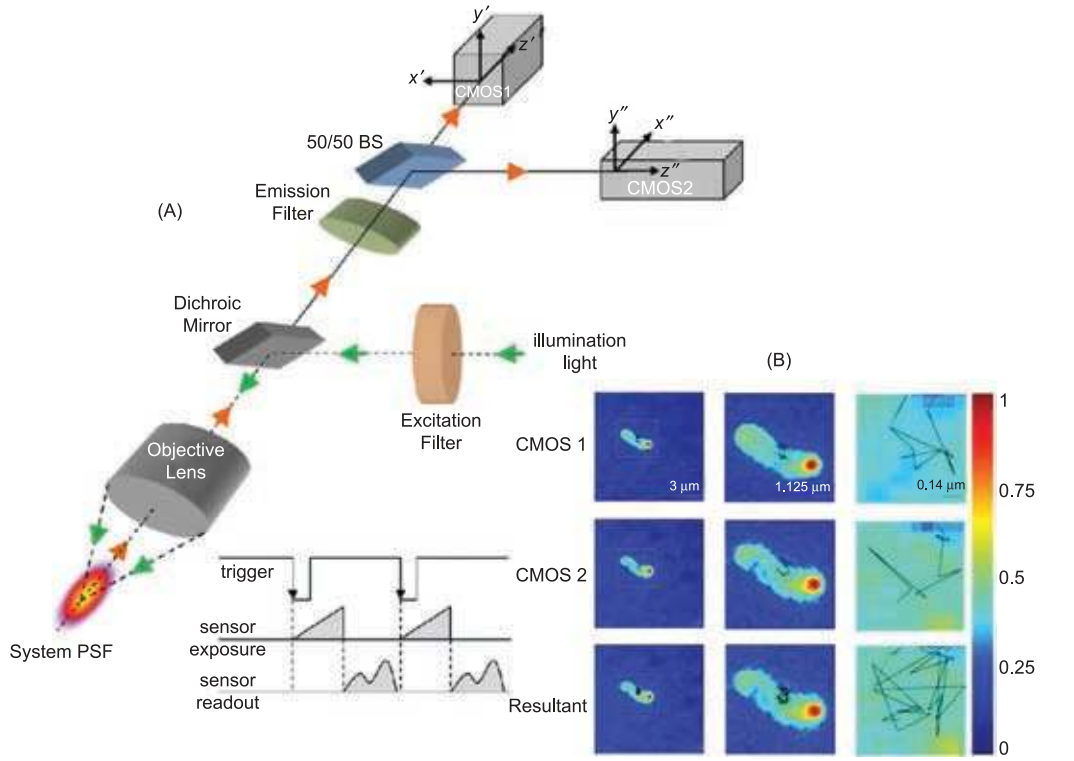

Figure 4: (A) Schematic diagram of the optical setup for the temporal resolution enhancement system. The timing diagram of the CMOS camera is also shown. Camera 1 acquires an image during the readout time of camera 2 and vice-versa, thus dynamically capturing images alternately. (B) Trajectory of E coli (coated with a single layer of NHS-Rhodamine dye) from CMOS cameras 1, 2 and temporally superresolved data. The boxed region indicated in the images is magnified to show the path taken by the E coli cell in the liquid medium.

resolution is improved as compared to widefield microscopes. This has significant application in biology, where a single plane of the specimen (say, cell) has to be imaged without losing the minute details due to fluorescence from neighboring planes and due to scattering effects.

Figure 5 shows the schematic of a confocal microscope. The basic concept of this technique is to scan the image by illuminating a smallest possible spot in the plane of focus. A monochromatic light is focused on a specimen at a certain depth. A laser beam is an ideal source as it contains all its energy in a collimated coherent plane wave. High numerical aperture (NA) of the objective lens is used to focus the light sharply at a single point.[34] The fluorescent signal emitted by the specimen is collected by the same objective. The pinhole is positioned before the detector to allow fluorescence only from the illumination region to reach the detector. The light source is then moved to the next point on the specimen and the image is acquired again. The plane of focus can also be changed with a computer-controlled stepper motor and optical sections can be acquired at different depths throughout the specimen. The images thus acquired are stacked together using a simple computational algorithm to generate a high-resolution volume of the specimen and therefore provide three-dimensional information of the specimen.

The point spread function (PSF) of the optical system defines its resolution. The effective PSF of a confocal system is given by[57]

$$K(x,y,z)=\left[\kappa(x,y)\otimes|h_{det}(x,y,z)|^2\right]\times|h_{ill}(x,y,z)|^2 \quad (6)$$

The first term in the equation is the effect of scanning through a finite sized pinhole which is a convolution of the detection PSF with the detection pinhole aperture, $k(x, y)$ in the focal region. h_{ill} and h_{det} are amplitudes of the illumination light and detection light respectively.

The system PSF for a typical confocal system is shown in Fig. 6. It may be noted that the size of the confocal PSF scales with pinhole dimension. Small pinhole rejects light even from the very nearest specimen layer. This is evident from the XZ planes of the system PSF (see, Fig. 6) corresponding to

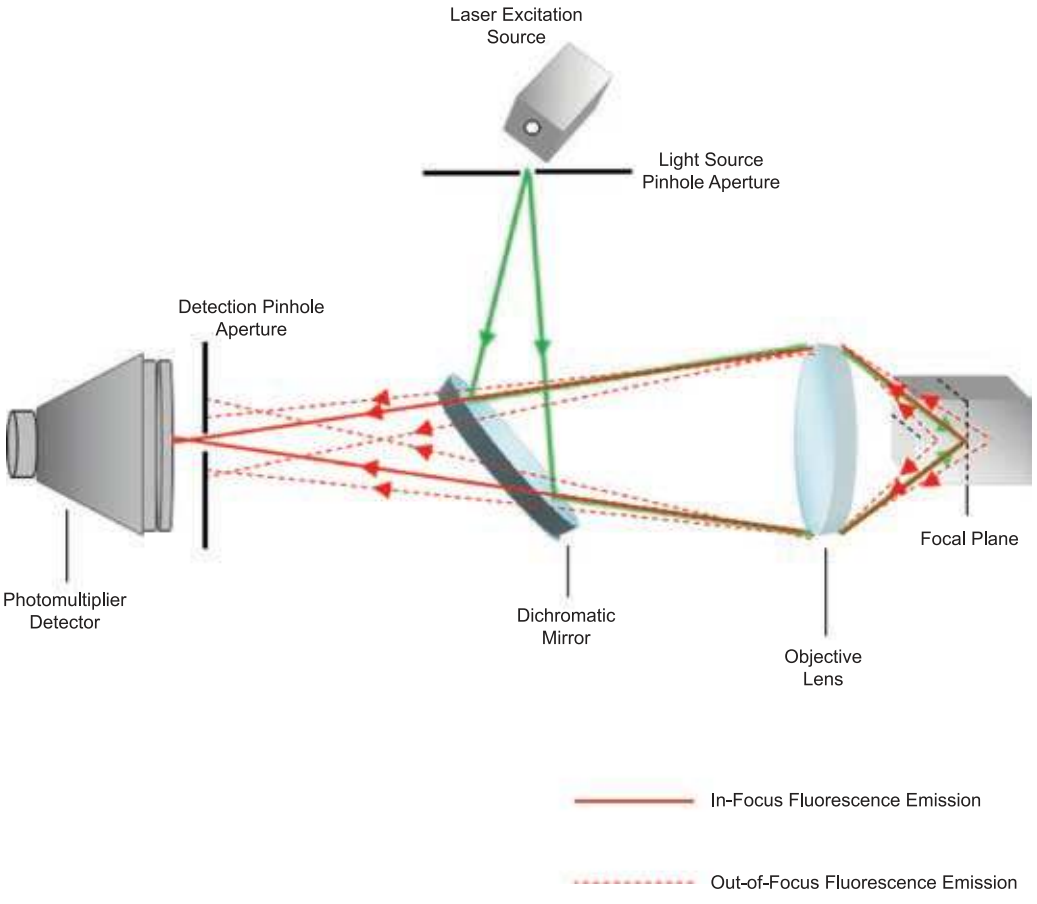

Figure 5: Schematic setup of a confocal microscope.

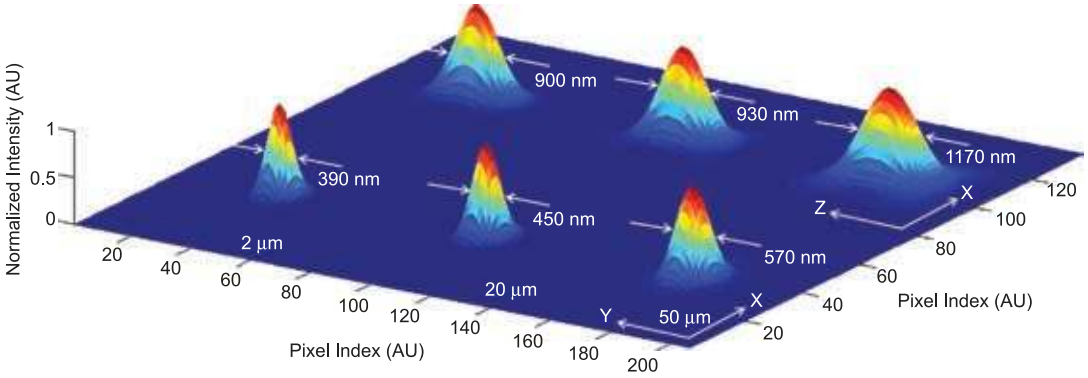

Figure 6: Lateral and axial PSF of a typical confocal microscope for varying pinhole size (2 µm, 20 µm and 50 µm).

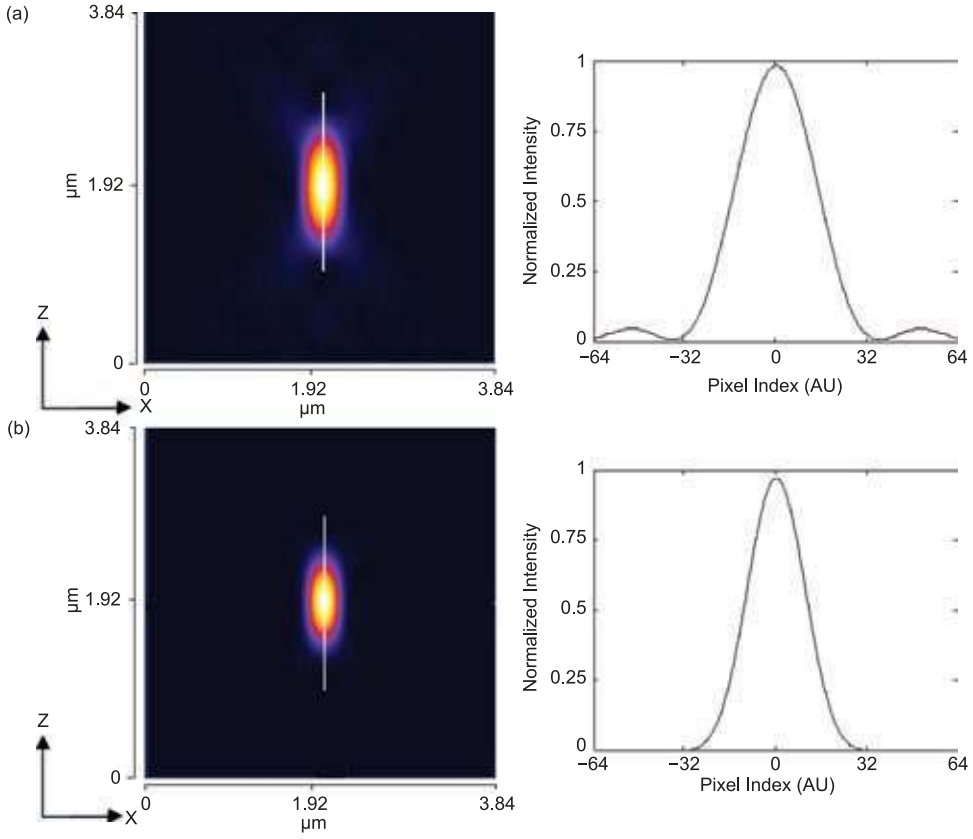

Figure 7: Comparison of the axial detection PSFs for widefield and confocal microscopes.

three different pinhole size (2 µm, 20 µm and 50 µm). This suggests that a compact and small PSF can be obtained for smaller pinhole. On the flip side, small pinhole reject a large portion of light, thereby signal falls off significantly. So, a balance needed to be maintained between SNR and size of the pinhole used.

The improvement of resolution can be understood by comparing the PSFs of the conventional widefield microscope to that of a confocal microscope (Figure 7). The axial resolution improvement for confocal microscope is evident as compared to the widefield axial PSF. In general, the diffraction effect tends to spread the image of a point object, and the PSF (which is a response of the imaging system to a delta function) describes this spreading. Confocal microscope achieves a theoretical axial resolution improvement of about $1/\sqrt{2}$ as compared to the widefield microscope.[35,16] Confocal microscope brings with

it several disadvantages that are not seen in widefield microscopes. One of the most important problems is photobleaching. The other problem is of scattering; when a confocal microscope is used to image a thick layer of specimen, the excitation and emission light travels through the volume where interaction with other molecules change the direction of light.

Fig. 8 show the images of Actin filaments obtained using both widefield epifluorescence and confocal fluorescence microscope. The Actin filaments are stained with Alexa Fluor Phallodin 488 dye which has an excitation and detection peak wavelength of 488 nm and 518 nm respectively. The epifluorescence microscope shows the distribution of Actin filaments in BPAE cells. Since the fluorescence is also detected from out-of-focus planes, the resulting image is blurry and it is difficult to resolve features. On the other hand, the confocal image is crisp primarily due to the fact that photons from off-focal planes are rejected by the pinhole. This further strengthens Confocal microscope as a potential 3D imaging modality.

1.3 *Light-sheet based fluorescence microscopy*

Light-sheet microscopy, as the name somewhat suggests, employs a sheet of light for illumination instead of a cone of light. The detection scheme generally employed is an orthogonal arrangement. This combination of illumination and detection schemes gives some what unique features such as, minimized photo-bleaching, reduced scattering and an inherent optical sectioning ability. Light-sheet based microscopy has been implemented in various forms, notably: Orthogonal-plane fluorescence optical sectioning (OPFOS),[22] 3D light scanning macrography,[36] Thin light-sheet microscope (TLSM),[37] Selective plane illumination microscopy (SPIM),[23] Ultramicroscopy,[39] Digital scanned laser light-sheet fluorescence microscopy (DSLM),[40] and Objective coupled planar illumination microscopy (OCPI).[41] In general, the axial resolution of conventional microscopes is inferior to the transverse resolution, and this fact adversely affects their ability to obtain high-resolution three-dimensional images. In an orthogonal detection scheme, the axial resolution of the system is essentially determined by the lateral resolution of the detection arm. This improves the axial resolution of the overall system.

The setup of SPIM, which is a typical light-sheet based microscopy technique, is described in Fig. 9. Light is made to converge within the sample, typically with the help of cylindrical optics and near the waist of such a convergent beam, it can be roughly considered as a planar sheet as shown in Fig. 9. Thickness of the light sheet can be adjusted from 1–10 μm, while the height and axial extent can span over several tens of micrometers.[42] We have also obtained similar experimental results for light-sheet generation with slightly elaborate optical setup and the results are presented in Fig. 10. This suggests a light sheet of thickness 12 μm and a width of 100 μm which is good for imaging large specimens.

Detection is carried out by an independent optical arm which is usually placed perpendicular to the illumination axis such that the focal plane of the detection objective coincides with the

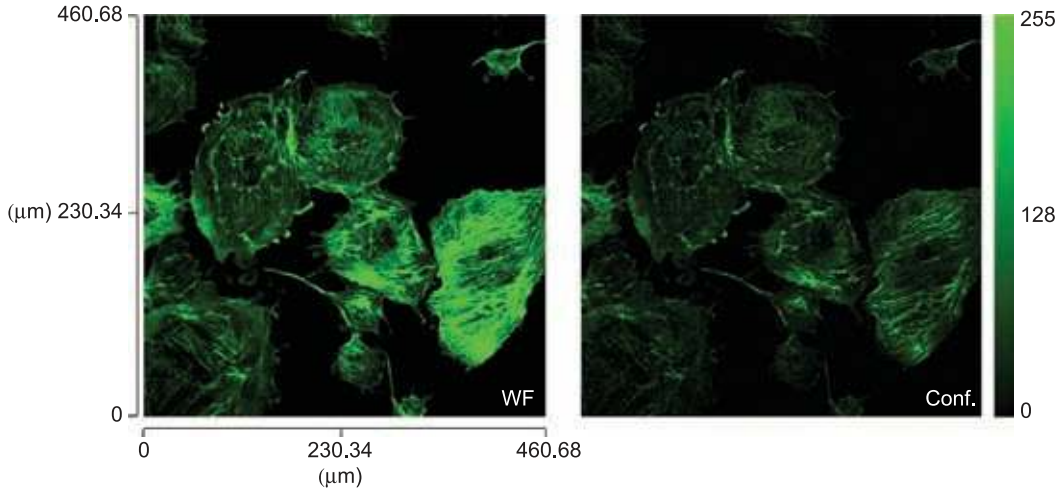

Figure 8: Images of Actin filaments (tagged with Alexa Fluor 488 phallodin) in BPAE cells obtained using epifluorescence and confocal microscopes.

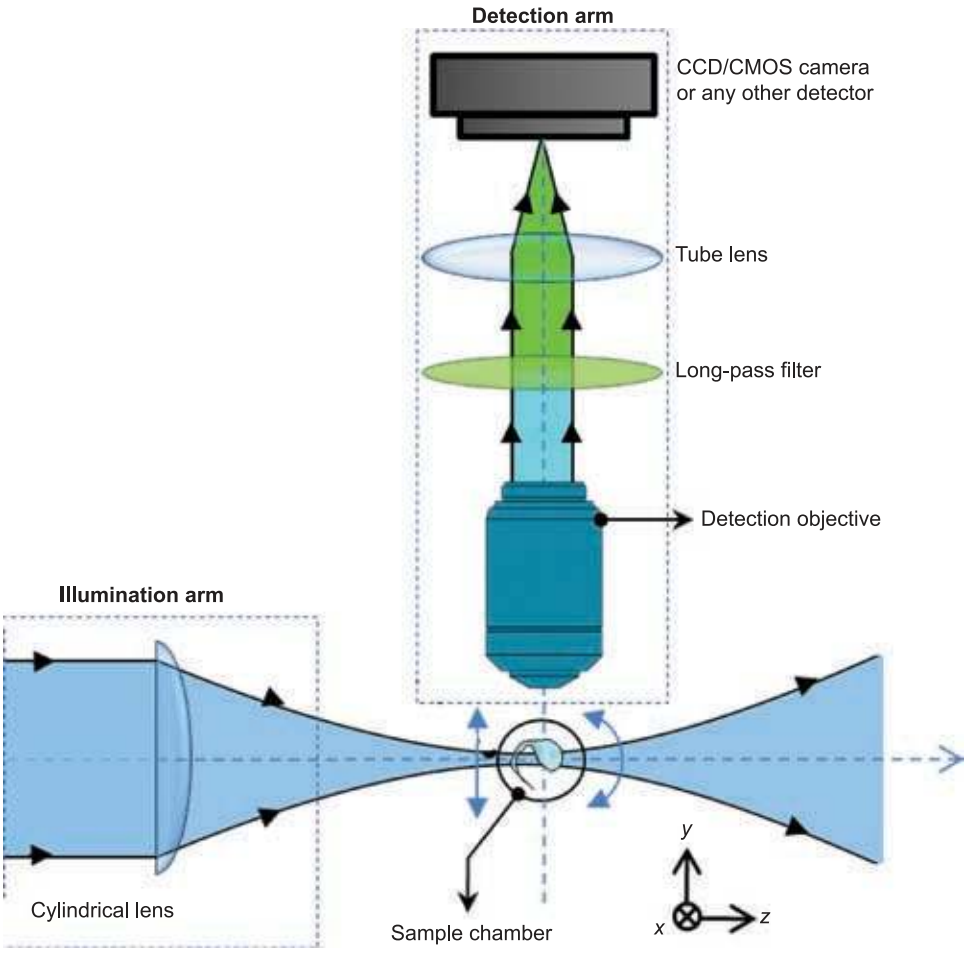

Figure 9: Schematic description of a typical SPIM setup.

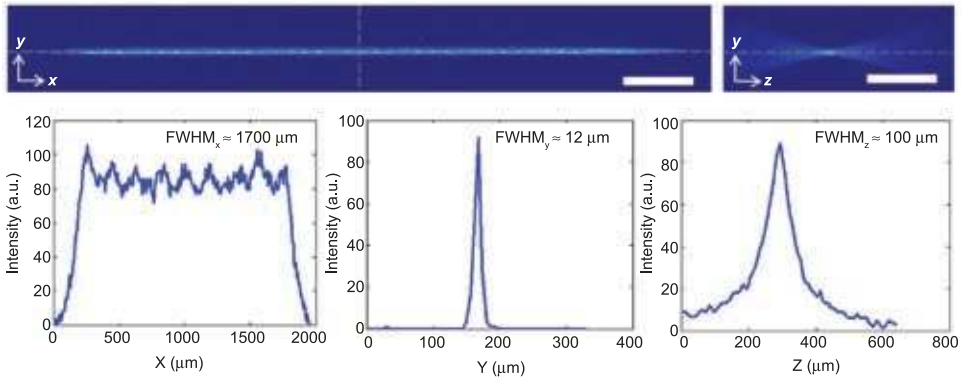

Figure 10: Experimentally obtained light point spread function of a light-sheet excitation scheme, generated with the help of cylindrical optics. The co-ordinate axes convention is the same as that of the previous figure hence the y-profile corresponds to the thickness of the sheet while x and z-profiles corresponds to the width and extent of the sheet respectively. Scale bar denotes 200 μm.

light-sheet. Some schemes can also employ dual camera detection system for high-speed image acquisition.[71] Filters serve the usual purpose of prohibiting the illumination light and stray light, thereby allowing only the light emitted by the fluorophores to be detected. An intuitive way of acquiring a complete 3-dimensional image of the sample volume is by translating the sample through the sheet and capturing many views to form an image stack. Such stacks can be acquired

for different orientations of the sample and finally combined computationally into an image volume of better quality known as multi-view reconstruction (MVR).[23]

The overall lateral resolution of SPIM is theoretically similar to that of epifluorescence microscopy but the overall axial resolution of the former can be much improved over the latter, provided that the light-sheet is made thinner than the axial resolution of the detection objective. Due to this enhanced axial resolution, optical sectioning is possible and photo-induced damages are reduced as discussed before. Since the detection arrangement is essentially a conventional wide-field microscope, light-sheet based microscopy techniques retain the capability of high speed imaging. All these factors combined together makes light-sheet microscopy a prime candidate in several applications such as developmental biology. For example, using SPIM, Huisken et al. demonstrated that embryogenesis of *Drosophilia* and *Medaka* can be studied by imaging them continuously for up to 3 days in vivo, at a depth of about 500 μm with a resolution of better than 6 μm.[38] Holekamp et al. used objective-coupled planar illumination (OCPI) microscopy to perform high-speed imaging studies (200 fps) to analyze pheromone-sensing neurons in mouse.[41] In 2008, DSLM technique was used by Keller et. al. to develop a comprehensive database for the first 24 hours of the development of mutant as well as wild-type zebrafish embryos.[40] This so called 'digital embryos' contain comprehensive information on cell division, positions and migratory tracks with an impressive temporal resolution of 1.5 billion voxels per minute. Fig. 11 show the images of *Lactobacillus* encaged in a Agarose gel-matrix. The bacteria was coated by fluorescent polymers using layer-by-layer technique. One can immediately notice larger field-of-view with a dark background which is the hallmark of single plane illumination. Given these multifarious applications and the astounding pace of their development, light-sheet based imaging techniques indeed present a promising future.

2 Multiphoton Fluorescence Microscopy

Multiphoton microscopy has brought in a sea change in the field of fluorescence microscopy. This has enabled many improvements in fluorescence imaging apart from the fact that this proves the fundamental aspect of possible high energy transition with low energy photons. Two-photon excitation occurs when two low energy photons combine together to produce a high energy transition. This can be explained by Jablonski energy diagram as shown in Fig. 1, where, the molecule absorbs two or more photons almost simultaneously to effect a transition to higher energy states S_n; $n > 0$. Since the probability of such transitions are rare, this requires high power pulse laser source.

There are many advantages of multiphoton excitation over single photon excitation process: 2PE enables pin-point excitation or high selectivity. This is due to the small two-photon excitation cross-section $\approx 10^{-50}$ cm^4 $s/photon$ which restricts the occurance of such rare events only at the focus. It is only the focus that has the highest photon density for such two-photon events to be possible. This is also the reason that, 2PE does not cause photobleaching at the top and bottom layers of the specimen, that is well-known to occur in single photon excitation microscopy. Other important applications of 2PE are in spectroscopy. Certain electronic states are not accessible by single-photon excitation primarily due to selection rules, but can be probed by multiphoton excitation. Moreover, two-photon excitation can excite fluorophores which are UV-active using visible light. As a consequence of this, 2PE reduces scattering by an increadible factor of λ^{-4}, thereby enabling depth-imaging. There are many more advantages of multiphoton over single photon. Here we discuss some of the widely used variants

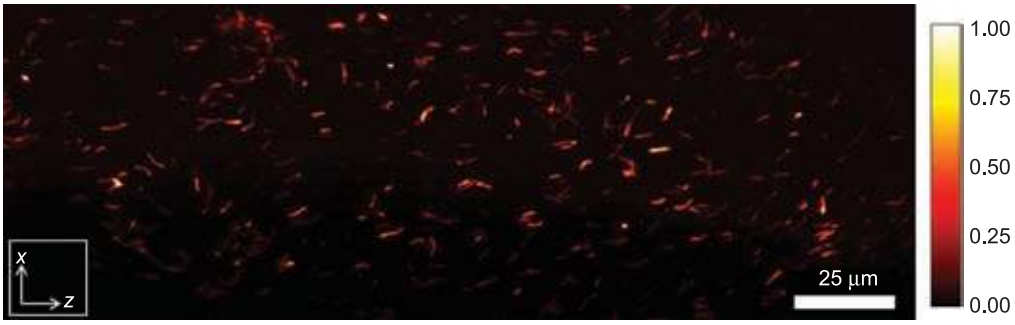

Figure 11: Light sheet images of dye-coated Lactobacillus trapped in an Agarose gel matrix.

of fluorescence microscopy techniques based on two-photon excitation process.

2.1 *Two photon laser scanning fluorescence microscopy*

This microscopy technique is inspired by the seminal work of Gueppert Mayor published in the year 1932.[4] Using quantum mechanical calculations, she could prove the striking fact that high energy transitions in molecules can be effected by using low energy light. This imposes certain conditions on the light-matter interactions such as, simultaneity of the photon absorption (photon absorption must take place within the dipole-transition time i.e, $<10^{-16}$ sec), very high photon density for compensating low molecular absorption cross-section and symmetry considerations.[63] In a nutshell, this means a very high photon flux of low energy is required which can be generated by pulsed laser. This is the reason that took almost 30 years to get the first experimental verification by Kaiser in 1961.[64] Specifically it took another 30 years for the first succcessful application in biological imaging by Denk et al. in 1990.[12] Thereafter, the field flourished at far greater pace than expected. It would not be possible to give all the theoretical flavour in this brief review. We refer to[62] and[63] for detailed theoretical derivation.

Since n-photon excitation results from the simultaneous absorption of n number of photons, the fluorescence intensity has the n-power dependence on the excitation intensity i.e,

$$I_f \propto I^n \Rightarrow I_f = \sigma_n I^n \tag{7}$$

where, the absorption cross-section σ_n is given by[76]

$$\sigma_n = \sigma_1^n \Delta^{n-1} \tag{8}$$

and σ_1 is the single-photon absorption cross-section.

Two-photon excitation microscopy is well characterized by the system PSF.[75] Because of the intensity-squared dependence, the excitation PSF for linearly-polarized light illumination is given by,

$$\begin{aligned} h_{ill}(u,v,\phi,\lambda_{ill}) &= |\bar{E}(u,v,\phi,\lambda_{ill})|^4 \\ &= \Big[I_{0,\lambda_{ill}}^2 + I_{2,\lambda_{ill}}^2 + 2I_{1,\lambda_{ill}} I_{2,\lambda_{ill}} \cos(2\phi) \\ &\quad + 4I_{1,\lambda_{ill}}^2 \cos^2\phi \Big]^2 \end{aligned} \tag{9}$$

The detection is the collection fluorescence light (stoke-shifted wavelength) by the same objective. So, the detection PSF is given by

$$\begin{aligned} h_{det}(u,v,\phi,\lambda_{det}) &= |\bar{E}(u,v,\phi,\lambda_{det})|^2 \\ &= |I_{0,\lambda_{det}}|^2 + 2|I_{1,\lambda_{det}}|^2 \\ &\quad + |I_{2,\lambda_{det}}|^2 \end{aligned} \tag{10}$$

The total system PSF for multiphoton microscopy is simply the product since, no pinhole is involved in two-photon excitation microscopy. So, the expression for system PSF is

$$h_{sys} = h_{ill}(u,v,\phi,\lambda_{ill}) \times h_{det}(u,v,\phi,\lambda_{det}) \tag{11}$$

where the diffraction integrals are as explained in Section 1.

Fig. 12 shows the excitation, detection and the system PSF for 2PE microscopy (all, XY, XZ and YZ planes). The excitation and emission wavelength are chosen to be 910 nm and 520 nm respectively. Comparatively, TPE excitation PSF is broader than one-photon variant because larger wavelength is employed for 2PE process. This is also evident from Abbes diffraction limit.[6] Fig. 13 shows the lateral XY plane and 3D images of Convalaria Majalis tissue section. In this case, the sample was excited at 750 nm and the fluorescence was detected at 675 nm.

2.2 *2-photon 4-pi microscopy*

The 4π geometry was first proposed by C. Cremer and T. Cremer signifying the maximal possible aperture angle for excitation and detection.[66] The first explanation of a workable system of 4Pi microscopy for biological imaging was proposed by Stefan Hell.[15,16] Based on the interference of the illuminated light, emitted light or both, the 4pi microscopes are classified as type A, B or C respectively. The 4π geometry is shown in Fig. 14. Light from both the objectives are made to interfere at the geometrical focus. This results in the interference pattern along the axial direction, consisting of a narrow central maximum with side lobes above and below the focal plane. The side lobes, which result from the partial solid angle of the superposing waves, can be as high as 30% of the main lobe.[67] During the same period, the first experimental demonstration of the two-photon laser scanning fluorescence microscope was achieved by Denk et al.[12]

Since two photon excitation process has an intensity-square dependence on the illumination intensity, the excitation PSF (A type) is given by the equation 12 (for linearly polarized light):

$$\begin{aligned} h_{ill}(u,v,\phi) &= |\mathbf{E}(u,v,\phi) + \mathbf{E}(-u,v,\phi)|^4 \\ &= [Re\{I_0\}^2 + Re\{I_2\}^2 \\ &\quad + 2Re\{I_1\}Re\{I_2\}\cos(2\phi) \\ &\quad + 4Re\{I_1\}^2 \cos^2\phi]^2 \end{aligned} \tag{12}$$

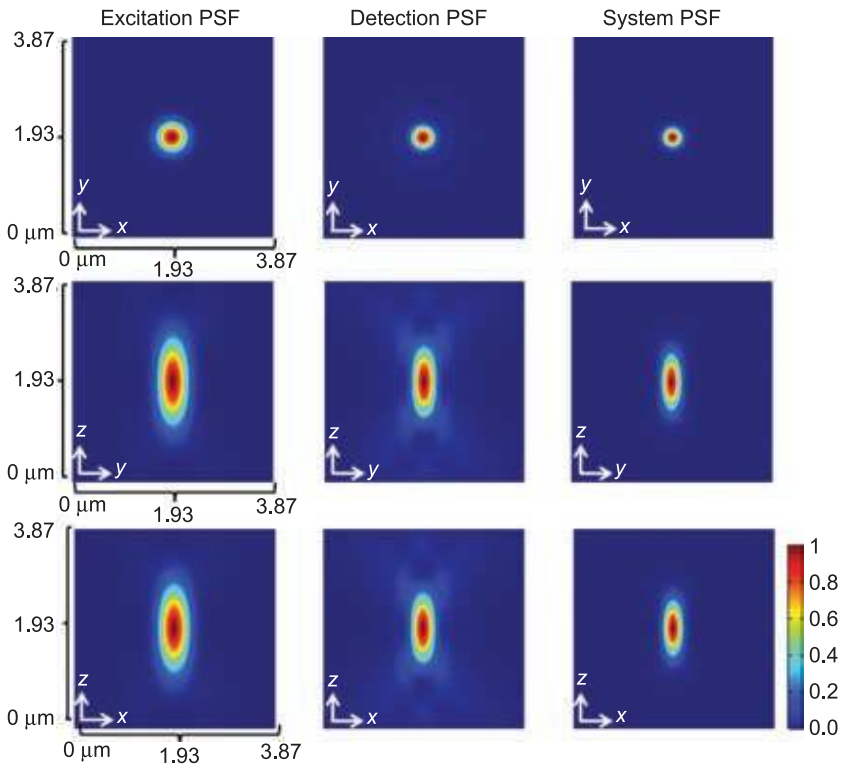

Figure 12: XY, XZ and YZ planes of excitation, detection and system PSF for 2PE microscopy.

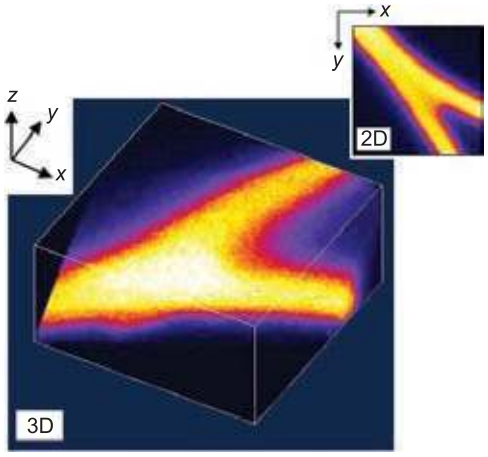

Figure 13: Images of *Convalaria Majalis* obtained using TPE microscopy.

For circularly polarized light, this simplifies to $h_{ill}(u,v,\phi) = [Re\{I_0\}^2 + 2Re\{I_1\}^2 + Re\{I_2\}^2]^2$.

Again, since the emitted photons are randomly polarized, the detection PSF is:

$$h_{det}(u,v,\phi) = |I_0|^2 + 2|I_1|^2 + |I_2|^2 \qquad (13)$$

Fig. 15 shows the system PSF for two-photon 4*pi* fluorescence microscopy. The aperture angle is chosen as 60°. Corresponding excitation and

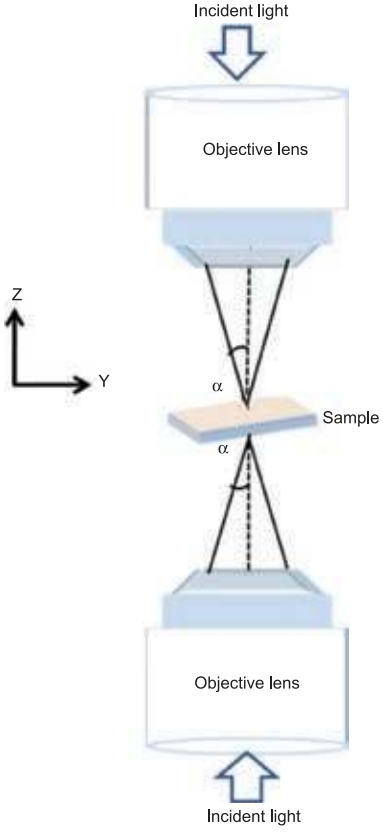

Figure 14: Schematic of the optical setup for 4-pi microscopy.

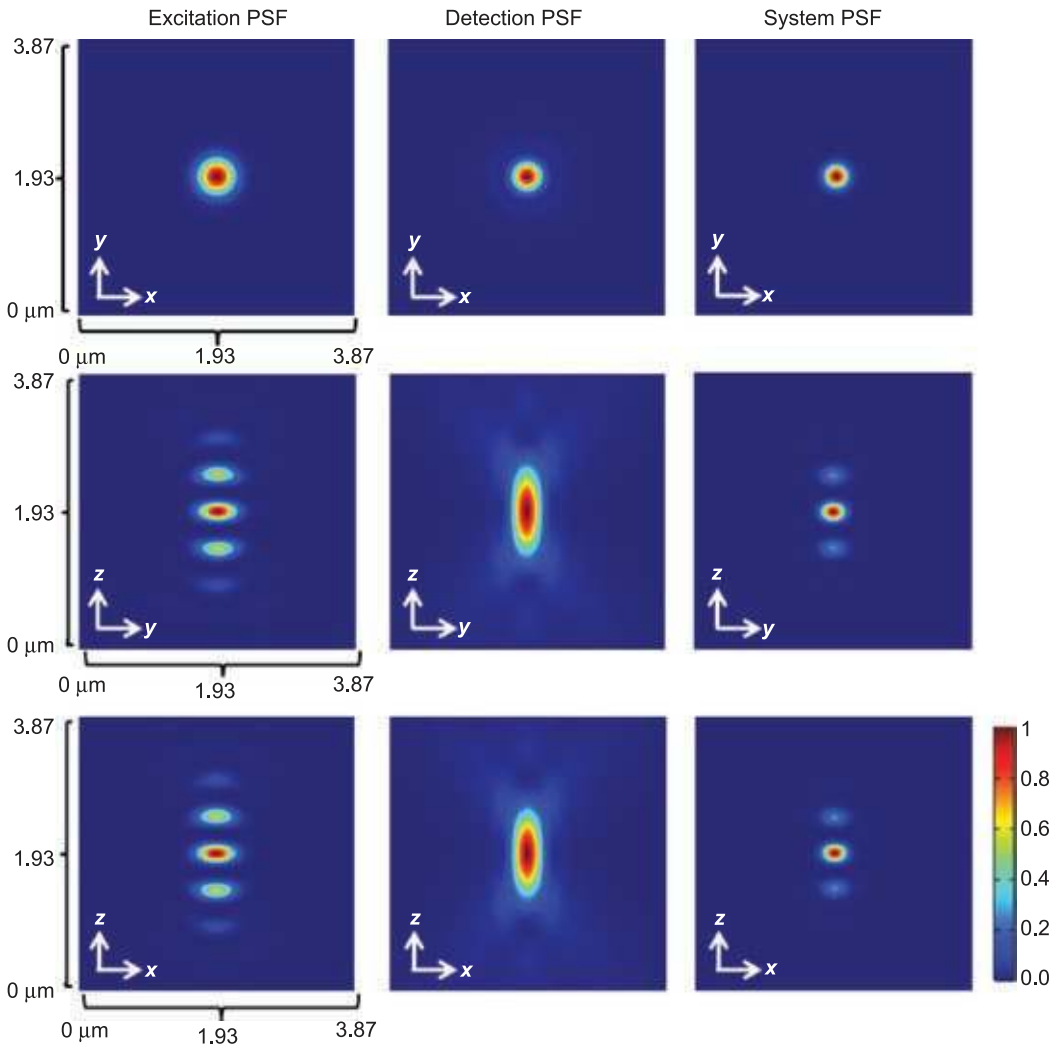

Figure 15: The *XY*, *YZ* and *XZ* planes of the (a) excitation, (b) detection and (c) system PSFs of two photon 4pi at an aperture angle of 60°. Simulation parameters λ_{exc} = 910 nm, λ_{det} = 520 nm.

detection wavelengths are chosen as λ_{exc} = 488 nm and λ_{det} = 520 nm respectively. The PSFs are evaluated on 128 × 128 × 128 grid with a sampling of 30 nm, which correspond to a physical dimension of 56.62 µm^3. The XY-, YZ-, and XZ-planes of the system PSF along with the excitation and detection PSF are shown in Fig. 15. The interference pattern in the excitation PSF is quite evident, which is a result of superposition of incoming waves from two objective lens (see, Fig. 14). The interference is ensured by phase matching between both the incoming wave derived from the same source. Since the detection is performed by a single lens, the detection PSF resembles that of epifluorescence system. Fig. 16 shows a comparison between the single-photon and two-photon variant of 4*pi*-type-A system. Side lobe suppression is quite evident in two-photon version, which is due to the inherent localization produced by intensity-squared relation. In the single photon version of 4*pi* microscopy, the sidelobes produce strong image-artifacts in the acquired images thereby giving a false impression of the presence of fluorophore. This can be seen in Fig. 17, which show distribution of mitocondrial network inside a cell where GFP fluorophore was used to tag the network. Close inspection shows that prominent dot-like features are accompanied by side-lobes. These sidelobes are artifacts due to the 4*pi*-PSF and should not be interpreted as part of fluorophore-active regions. To some extent, the effect can be minimized by image deconvolution and statistical image reconstruction methods.[68–70] In the last section (Section 4), we will discuss statistical image reconstruction technique to address the side-lobe

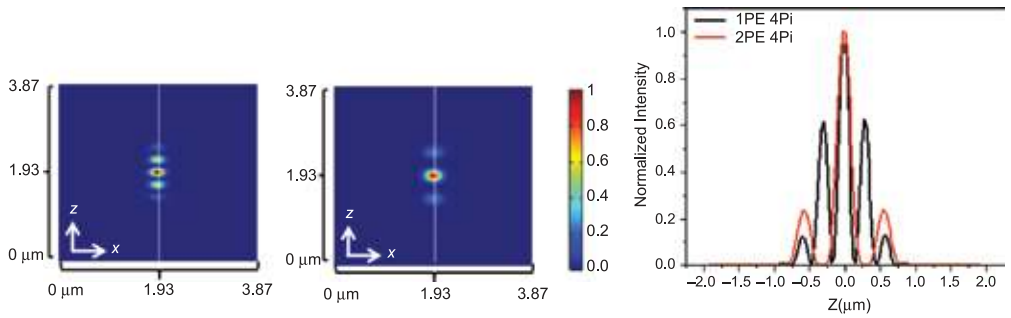

Figure 16: System PSF and intensity profile for single and two photon for the aperture angle 60°.

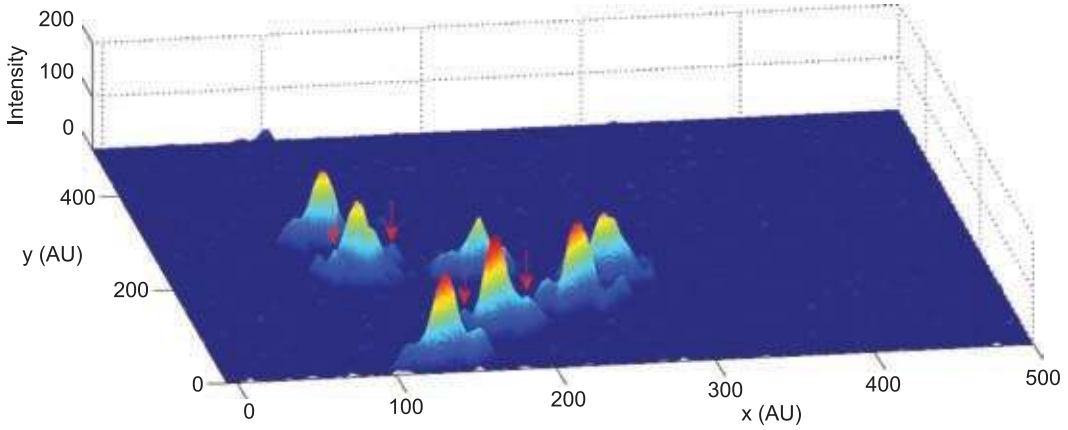

Figure 17: 4pi image (surface plot) of the mitocondrial network tagged with GFP.

issue and more importantly to develop statistical techniques to suppress the noise.

3 Super Resolution Fluorescence Imaging Techniques

In this section, we will very briefly go through the super-resolution imaging techniques. It may be noted that there are a quite a few review articles and book chapters that gives a detailed information,[16,77] so we will briefly go through these techniques. Broadly super-resolution techniques can be categorized into two types: (1) Based on PSF Engineering and (2) Based on photophysics of the probe molecules.

3.1 *Stimulated Emission Depletion (STED) microscopy*

STED microscopy reduces the system PSF by a combination of traditionally used Gaussian beam and an additional Donut shape STED beam. STED falls in the first category which is predominantly PSF engineering. The specimen is illuminated by two synchronized ultrafast pulsed laser sources: Excitation laser pulse which has a Gaussian beam profile, and wavelength-shifted depletion pulse laser with a donut profile. The pulse duration of both the lasers are generaly in pico-seconds with excitation pulse being of shorter duration. It may be noted that, pulse lasers are cleverly chosen to be close to time-scales of molecular relaxation. Both the Gaussian and Donut beams remain diffraction limited. The STED pulse is generated by an appropriate phase-modulator so as to make sure that the zero-intensity appears at the center with exponentially growing intensity as we move towards the periphery. This results in a Donut-shaped beam. The wavelength and duration of the STED beam pulse are appropriately chosen so as to coincide with the emission maximum and saturation intensity of the dye.

The dye is initially excited by a diffraction-limited Gaussian beam pulse. This results in the excitation of all the molecules to the singlet excited state. Then, this is immediately followed by another pulse with a Donut-shaped beam that surrounds the central focal point of the excitation beam. Note, the beam is slightly wavelength-shifted towards red. So, all the fluorophores except at the central region undergoes stimulated depletion, thereby leaving out fluorophores at the center to undergo spontaneous emission i.e, fluorescence. This results in a very compact effective PSF. In order to obtain a complete 3D image, the

effective PSF is raster scanned across the specimen and 3D image is constructed.

A very interesting recent development in STED is the integration of STED in a 4π-geometry. This is termed as iso-STED.[65] This adds the advantage of highest lateral resolution (obtained from STED part) with that of highest axial resolution(obtained by 4pi part). This combination is a complete realization of truely nanoscale imaging modality. The resolution of such an imaging technique has approached few tens of nanometers.[16] Although, the biggest concern has been the photobleaching caused by high-power laser beam, this technique is growing fast and continues to impress.

3.2 *Localization microscopy*

Localization microscopy falls in the second category where photophysical properties of the fluorophore is exploited to render super-resolution. These properties are mainly photo-switching, photo-activation and triplet-state transition rate. All the localization techniques exploit these properties to control the number of excited molecules. The mechanisms responsible for ON-OFF transitions are photoisomerization, electron transfer or triplet state formation. Because of this, a sparse subset of molecules can be continously toggled between the bright and dark states.

Some of the well-known localization techniques are PALM, STORM, fPALM, GSDIM and IML-SPIM. The basic philosophy behind these techniques is the ability to excite a sparse subset of fluorophores from a dense ensemble. Here, sparse subset means distances exceeding Abbe's resolution limit. The advantage of this technique is that no modification of the optical setup is required. It is advisable that, this be implemented on wide-field and total internal reflection fluorescence optical microscope platforms for best results.

The sequential steps involved in localization microscopy are: (1) Switching ON the fluorophores in a sparse subset of the ensemble, and (2) The determination of the coordinates (centroid) of the molecule by fitting the PSF to a Gaussian function, and (3) Switching-OFF so that they cannot re-participate in the reconstruction process. It may be noted that single-molecule blinking is a stochastic event. Upon excitation with a low power activation laser, a small sparse percentage of fluorophores are stochastically switched ON. They are then localized and then photobleached to remove from the ensemble. This is performed for large number of times to collect enough single molecule signatures for bringing out the super-resolved structure of the specimen.

The idea behind localization techniques is that the position of a single molecule can be localized depending upon the photons collected provided there is no similar marker within the diffraction limit. The localization precision σ has contributions from photon counting noise, pixilation noise and background noise as shown by the following expression,[74]

$$\sigma^2 = \frac{s^2}{N} + \frac{a^2}{12N} + \frac{8\pi s^4 b^2}{a^2 N^2}, \tag{14}$$

where N is the number of photons collected, s is the standard deviation of the Gaussian intensity PSF, a represents the effective pixel size, and b is the background noise. For best results, an EMCCD camera is recommended.

4 Statistical Image Reconstruction for Fluorescence Microscopy

Deconvolution and statistical methods play pivotal role in fluorescence imaging.[57,72] Specifically for low-light imaging, statistical methods are preferred over deterministic methods (such as, Image Devonvolution). Here we discuss statistical methods that are more general and are hence applicable for both low and high SNR images.

In a fluorescence imaging system, the image g_0 is a linear superposition of the values of f_0 and K. Mathematically, this is represented as $g_0 = K * f_0$ where K is the impulse response function or the Point Spread Function (PSF) of the imaging system. The diffraction-limited PSF passes the low-frequency content in the object and restricts the high spatial frequencies, thereby resulting in blurring. The image is severely corrupted by noise thereby, further degrading the quality of the acquired image. The image generation in a fluorescence microscopy can be mathematically approximated as

$$g(x,y) = K(x,y) * f(x,y) + \eta(x,y) \tag{15}$$

Since the image is degraded by addition of noise and blurring, there arises a need to have techniques to recover the object from the degraded image. This is an inverse problem, and turns out to be ill-posed. In an inverse problem, the data is always affected by noise which is a small random oscillation. The solution method would amplify the noise producing large oscillations in the image.[72] This implies that there are many approximate solutions which reproduce the data within a given noise level. A standard approach for addressing this problem of ill-posedness is provided by the regularization theory.[72]

Here, we focus our attention to the case where the noise follows Poisson distribution. For ML approach, the true estimate of the object is obtained based on the knowledge of the system

point spread function (PSF). Photon emission in fluorescence microscopy is known to obey the Poisson distribution and as a result the photon detection is Poissonian as well. The likelihood function which is the probability of observing the measured data g given the object f is

$$L(f) = P(g \mid f) = \prod_{m=0}^{N} e^{-(Af)_m} \frac{(Af)_m^{g_m}}{g_m!} \tag{16}$$

where, f is the mean value of the random variable and g is the recorded data set. The mean of the distribution function is $Af = K * f$, K being the PSF of the imaging system. We have also used the fact that emission from each pixel is an independent event.

Expectation maximization algorithm, first proposed by Dempster in 1977[58] offers a numerical method for determining the maximum likelihood estimate (MLE). Shepp and Vardi, in 1982[59] introduced ML-EM algorithm for image reconstruction and the algorithm has remained a basis for most of the statistical reconstruction algorithms. In ML approach, the likelihood function is maximized to obtain the best estimate of the object. This is an iterative method where every reconstructed image is obtained from the previous iteration estimates.[72,59–61]

$$f_n^{k+1} = f_n^k \left(A^T \frac{g}{Af^k} \right)_n \tag{17}$$

This ill-posed problem can be bettered if one can introduce prior information in the image reconstruction problem. ML algorithm, however, suffers from dimensional instability at large iterations, producing noisy artifacts. ML does not support the incorporation of prior knowledge in the image reconstruction process. This restriction can be lifted by the introduction of Bayes theorem that relates the posterior distribution $P(f \mid g)$ with likelihood function $P(g \mid f)$ and prior distribution function $P(f)$,

$$P(f \mid g) = \frac{P(g \mid f)P(f)}{P(g)} \tag{18}$$

The determination of prior distribution is possible by approximately modeling the image field. One intutive way of modeling is to consider the fact that image field is smooth, i.e, a pixel in the image field is mostly affected by the neighborhood pixels. This brings in the concept of Markov Random Field.[43] Once image field is modeled as MRF, the image distribution is given by Gibbs distribution as per the Hammersley-Clifford theorem,[45]

$$P(f) = \frac{1}{Z}\ e^{-\frac{1}{\beta}\sum_n \sum_{j \in N_n} V(f_n, f_j)} \tag{19}$$

where, Z is the normalizing constant, β is Gibbs hyper-parameter, and $V(f_n, f_j)$ is the potential at the current pixel n due to the pixels f_j in the neighborhood ($j \in N_n$).

Solving the optimization problem for MAP (i.e, $\tilde{f} = \max_{f>0}[\log P(g \mid f) + \log P(f)]$) and using successive approximation, we get an iterative scheme to obtain the best possible estimate,[46]

$$f_n^{k+1} = \frac{f_n^k}{\sum_{m=1}^{M} A_{mn} + \frac{1}{\beta}\frac{\partial}{\partial f_n}\sum_{j \in N_n} w_{n,j} V(f_n, f_j)|_{f=f^k}} \times \left(A^T \frac{g}{Af^k} \right) \tag{20}$$

Over the years a large number of potential functions have been suggested in the literature to accurately model the prior function. One such simple yet effective potential function is quadratic potential.[44,51,53–55] Other potential functions are: Huber potential,[56] Cosh potential function,[44] Fuzzy potential function[47,48] and blind deconvolution.[50,49]

There are many ways one can study the characteristics of these iterative algorithms and their convergence. The readers can refer to excellent articles for better understanding of these properties.[44,72] In this brief review, we will rather focus on the simpler versions of MAP algorithm and compare it with ML algorithm. We have chosen to work with both synthetic and real data. Fig. 18, first column shows the synthetic data of three merging spheres (shown in gray scale) and two set of real data (false colored). The real data set are obtained using confocal laser scanning microscope of Yeast cell samples in which mitochondria is tagged with MitoTracker Orange CMX-Ros (Invitrogen Inc.) and Actin filaments in BPAE cells. It is evident that both ML and MAP algorithms produce high quality reconstruction. ML image is little noisier than MAP reconstructed images, which is due to the effect of quadratic potential that produces smoothing effect. Moreover, intensity plots show that both ML and MAP algorithms are capable of bringing out high-resolution features such as edges. Specifically, the background noise is substantially smoothened in the MAP reconstruction. This is

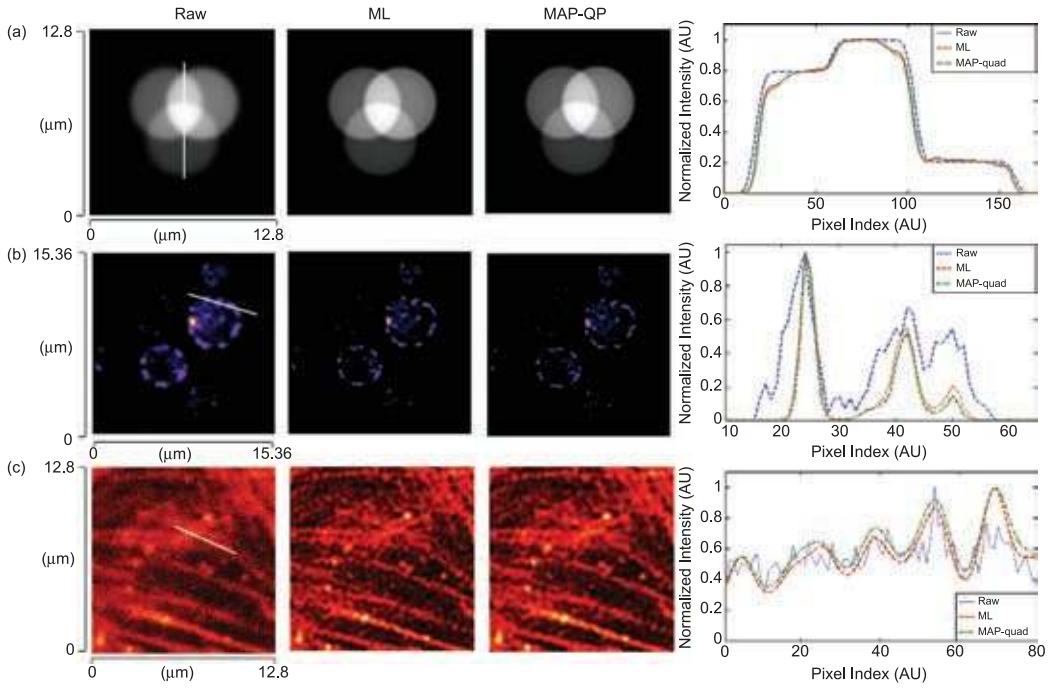

Figure 18: ML and MAP quadratic potential reconstruction of, (a) Simulated data, (b) Mitocondria tagged yeast cells, and (c) Factin filaments of BPAE cells.

possible because both the algorithms are based on statistical models.

Through this brief review, we propose to bring out some of the state-of-art and powerful techniques in fluorescence microscopy. The applications of these techniques are not limited to a specific branch of science and technology, it is expanding rapidly toinclude diverse disciplines such as food inspection, medical diagnostics and non-destructive imaging. There is a lot of scope for these optical microscopy techniques in the coming years especially at the interface of merging disciplines specifically, physics and biology.

Acknowledgement

The financial support from BRNS (under, DAE Young Scientist Research Award Scheme) and DST (under DST Fast Track Scheme) to is highly acknowledged.

Received 6 February 2013.

References

1. Herschel, J.F.W. On a case of superficial color presented by a homogeneous liquid internally colorless, Phil. Trans. Roy. Soc. (London), 135: 143–145 (1845).
2. Stokes, G.G. On the change of refrangibility of light, Phil. Trans. R. Soc. (London), 142: 463–562 (1852).
3. Jablonski, A. Uber den Mechanisms des photolumineszenz von farbstoffphosphoren, Z. Phys., 94: 38–46 (1935).
4. Gopert-Mayer, M. Uber elementarakte mit zwei quantensprungen, Ann. Phys. (Leipzig), 9: 273–294 (1931).
5. Abbe, E. Beiträge zur Theorie des Mikroskops und der mikroskopischen Wahrnehmung, Schultzes Arc. f. Mikr. Anat. 9: 413–468 (1873).
6. Abbe, E. Note on the proper definition of the amplifying power of a lens or a lens-system, J. Royal Microsc. Soc. 4: 348–351 (1884).
7. Minsky, M. U.S. Patent No. 3013467, Microscopy Apparatus, (1957).
8. Sheppard, C.J.R. and Choudhury, A. Image formation in the scanning microscope, Optica 24: 1051 (1977).
9. Sheppard, C.J.R., Gannaway, J.N., Walsh, D. and Wilson, T. Scanning Optical Microscope for the Inspection of Electronic Devices, Microcircuit Engineering Conference, Cambridge, (1978).
10. Brakenhoff, G.J., Blom, P. and Barends, P. Confocal scanning light microscopy with high aperture immersion lenses, J. Microsc. 117: 219–232 (1979).
11. Inoué, S. and Inoué, T.D. Direct-view high-speed confocal scanner—the CSU-10. In: Cell Biological Applications of Confocal Microscopy, 2nd ed. (B. Matsumoto, ed.), Academic Press, San Diego, 87–123, (2002).
12. Denk, W., Strickler, J.H. and Webb, W.W. Two-photon laser scanning fluorescence microscopy, Science 248: 73–76 (1990).
13. Hell, S.W. and Stelzer, E.H.K. Fundamental improvement of resolution with a 4Pi-confocal fluorescence microscope using two-photon excitation, Opt. Commun. 93: 277–282 (1992).

14. Hell, S.W., Schmidt, R. and Egner, A. Diffraction-unlimited three-dimensional optical nanoscopy with opposing lenses, Nature Photonics 3: 381–387 (2009).
15. Hell, S.W. and Wichmann, J. Breaking the diffraction resolution limit by stimulated emission: stimulated-emission-depletion fluorescence microscopy, Opt. Lett. 19: 780–782 (1994).
16. Hell, S.W. Far-Field Optical Nanoscopy, Science 316: 1153–1158 (2007).
17. Gustafsson, M.G.L. Nonlinear structured-illumination microscopy: Wide-field fluorescence imaging with theoretically unlimited resolution. Proceedings of the National Academy of Sciences 102(37): 13081–13086 (2005).
18. Betzig, E. et al. Imaging Intracellular Fluorescent Proteins at Nanometer Resolution. Science 313(5793): 1642–1645 (2006).
19. Rust, M., Bates, M. and Zhuang, X. Sub-diffraction-limit imaging by stochastic optical reconstruction microscopy (STORM). Nature Methods 3(10): 793–796 (2006).
20. Hess, S., Giririjan, T. and Mason, M. Ultra-High Resolution Imaging by Fluorescence Photoactivation Localization Microscopy, Biophysical Journal 91(11): 4258–4272 (2006).
21. Folling, J. et al. Fluorescence nanoscopy by ground-state depletion and single-molecule return, Nature Methods 5(11): 943–945 (2008).
22. Voie, A.H., Burns, D.H. and Spelman, F.A. Orthogonal-plane fluorescence optical sectioning: three-dimensional imaging of macroscopic biological specimens. J. Microsc. 170: 229–236 (1993).
23. Huisken, J., Swoger, J., DelBene, F., Wittbrodt, J. and Stelzer, E.H.K. Optical sectioning deep inside live embryos by selective plane illumination microscopy. Science 305: 1007–1009 (2004).
24. Thomas, A., Planchon, Liang Gao, Daniel E., Milkie, Michael W. Davidson, James A. Galbraith, Catherine G. Galbraith and Eric Betzig. Rapid three-dimensional isotropic imaging of living cells using Bessel beam plane illumination, Nature Methods 8: 417–423 (2011).
25. Florian O. Fahrbach and Alexander Rohrbach. Propagation stability of self-reconstructing Bessel beams enables contrast-enhanced imaging in thick media, Nature Communications 3: 632 (2012).
26. Purnapatra, S.B., Bera, S. and Mondal, P.P. Spatial filter based Bessel-like beam for improved penetration depth imaging in fluorescence microscopy, Scientific Reports (NPG) 2: 692 (2012).
27. Stephens, D.J. and Allan, V.J. Light microscopy techniques for live cell imaging, Science, 300: 82–86 (2003).
28. Brakenhoff, G.J., van der Voort, H.T.M., van Spronsen, E.A., Linnemans, W.A.M. and Nanninga, N. "Three-dimensional chromatin distribution in neuroblastoma nuclei by confocal scanning laser microscopy", Nature, 317: 748–749 (1985).
29. Wilson, T. 'Confocal Microscopy', Academic Press, London, (1990).
30. Fine, A., Amos, W.B., Durbin, R.M. and McNaughton, P.A. Confocal microscopy: Applications in neurobiology, Trends in Neuroscience, 11: 346–351 (1988).
31. Michiel Muller, Introduction to Confocal fluorescence Microscopy, SPIE-The International Society for Optical Engineering, (2006).
32. White, J.G., Amos, W.B. and Fordham, M. An evaluation of confocal versus conventional imaging of biological structures by fluorescence light microscopy, J. Cell Biol., 105: 41–48 (1987).
33. Carlsson, K., Danielsson, P., Lenz, R., Liljeborg, A., Majlof, L. and Aslund, N. "Three-dimensional microscopy using a confocal laser scanning microscope", Opt. Lett., 10: 53–55 (1985).
34. Jose-Angel Conchello and Jeff W. Lichtman. Optical sectioning microscopy, Nature Methods, 2: 920–931 (2005).
35. Wu, Q., Merchant, F.A. and Castleman, K.R. Microscopic Image Processing, Elsevier, (2008).
36. Huber, D., Keller, M. and Robert, D. 3D light scanning macrography, Jl. Microsc., 203: 208–213 (2001).
37. Fuchs, E., Jaffe, J.S., Long, R.A. and Azam, F. Thin laser light sheet microscope for microbial oceanography, Opt. Express, 10: 145–154 (2002).
38. Huisken, J., Swoger, J., Del Bene, F., Wittbrodt, J. and Stelzer, E.H.K. Optical sectioning deep inside live embryos by selective plane illumination microscopy, Science, 305: 1007–1009 (2004).
39. Dodt, H.U., Leischner, U., Schierloh, A., Jährling, N., Mauch, C., Deininger, K., Deussing, J.M., Eder, M., Zieglgänsberger, W. and Becker, K. Ultramicroscopy: three-dimensional visualization of neuronal networks in the whole mouse brain, Nat. Methods, 4: 331–336 (2007).
40. Keller, P.J., Schmidt, A.D., Wittbrodt, J. and Stelzer, E.H.K. Reconstruction of zebrafish early embryonic development by scanned light sheet microscopy, Science, 322: 1065–1069 (2008).
41. Holekamp, T.F., Turaga, D. and Holy, T.E. Fast three-dimensional fluorescence imaging of activity in neural populations by objective-coupled planar illumination microscopy, Neuron, 57: 661–672 (2008).
42. Engelbrecht, C.J. and Stelzer, E.H.K. Resolution enhancement in a light-sheet-based microscope (SPIM), Opt. Lett., 31: 1477–1479 (2006).
43. Geman, S. and Geman, D. Stochastic Relaxation, Gibbs Distributions, and the Bayesian Restoration of Images, IEEE Patt. Anal. Mach. Intell., 6: 721 (1984).
44. Green, P.J. Bayesian reconstructions from emission tomography data using a modified EM algorithm, IEEE Med. Img., 9: 84–93 (1990).
45. Besag, J. "Spatial interaction and the statistical analysis of lattice systems", Journal of the Royal Statistical Society. Series B (Methodological) 36: 192–236 (1974).
46. Mondal, P.P., Giuseppe Vicidomini and Diaspro, A. Markov Random Field Aided Bayesian Approach for Image Reconstruction in confocal microscopy, Journal of Applied Physics, 102: 044701 (2007).

47. Mondal, P.P. and Rajan, K. Fuzzy Rule based Image Reconstruction for Positron Emission Tomography, Journal of Optical Society of America A, 22: 1763–1771 (2005).
48. Mondal, P.P. Positron emission tomographic map reconstruction using fuzz-median filter, Applied Physics Letters, 89: 153903 (2006).
49. Wu, Q., Merchant, F.A. and Castleman, K.R. Microscopic Image Processing, Elsevier, (2008).
50. Giuseppe Vicidomini, Roman Schmidt, Alexander Egner, Stefan Hell and Andreas Schönle. Automatic deconvolution in 4Pi-microscopy with variable phase, Opt. Exp., 18: 10154–10167 (2010).
51. Verveer, P.J., Gemkow, M.J. and Jovin, T.M. A comparison of image restoration approaches applied to three-dimensional confocal and wide-field fluorescence microscopy, J. Microsc., 193: 50 (1999).
52. Joshi, S. and Miller, MI. Maximum a posteriori Estimation with Good's Roughness for Optical-Sectioning Microscopy, Journal of the Optical Society of America, 10(5): 1078–1085 (1993).
53. Mondal, P.P. and Rajan, K. "Fuzzy-rule-based image reconstruction for positron emission tomography", J. Opt. Soc. Am. A, 22: 1763–1771 (2005).
54. Zhou, Z., Leahy, R.M. and Qi, J. "Approximate maximum likelihood hyperparameter estimation for Gibbs priors", IEEE Trans. Image Process., 6: 844–861 (1997).
55. Alenius, S. and Ruotsalainen, U. "Generalization of median root prior reconstruction", IEEE Trans. Med. Imaging, 21: 1413–1420 (2002).
56. Huber, P.J. Robust Statistics, Wiley, (1981).
57. Bertero, M., Boccacci, P., Brakenhoff, G.J., Malfanti, F. and van der Voort, H.T.M. J. Microscopy, 157: 3–20 (1990).
58. Dempster, A., Laird, N. and Rubin, D. "Maximum likelihood from incomplete data via the EM algorithm", Journal of the Royal Statistical Society, 39: 1–38 (1977).
59. Shepp, L. and Vardi, Y. Maximum Likelihood Reconstruction for Emission Tomography, IEEE Trans Med Imaging, MI-1: 113–122 (1982).
60. Richardson, W.H. Bayesian-Based Iterative Method of Image Restoration, J. Opt. Soc. Am., 62: 55–59 (1972).
61. Lucy, L.B. An iterative technique for the rectification of observed distributions, Astron. Jl., 79: 745–765 (1974).
62. Diaspro, A. Confocal and Two-Photon Microscopy: Foundations, Applications and Advances, Wiley, New York, (2002).
63. Masters, B.R. and Peter T.C. So, Handbook of Biomedical Nonlinear Optical Microscopy, Oxford University Press (2008).
64. Kaiser, W. and Garrett, C.B.G. Two-photon excitation in CaF2: Eu2+, Phys. Rev. Lett. 7: 229–231 (1961).
65. Roman Schmidt, Christian A. Wurm, Stefan Jakobs, Johann Engelhardt, Alexander Egner and Stefan W. Hell, Spherical nanosized focal spot unravels the interior of cells, Nature Methods-5: 539–544 (2008).
66. Cremer, C. and Cremer, T. Considerations on a laser scanning microscope with high resolution and depth of field, Microsc. Acta, 81: 31–44 (1978).
67. Sylvia Glaschick, Carlheinz Röcker, Karen Deuschle, JörgWiedenmann, Franz Oswald, Volker Mailänder and Ulrich Nienhaus G. Axial Resolution Enhancement by 4Pi Confocal Fluorescence Microscopy with Two-Photon Excitation, Jl. Biol. Phys, 33: 433–443 (2008).
68. Schrader, M., Hell, S.W. and van der Voort, H.T.M. Three-dimensional super-resolution with a 4Pi-confocal microscope using image restoration, J Appl. Phys, 84: 4033 (1998).
69. Mondal, P.P. and Diaspro, A. Reduction of higher-order photobleaching in two-photon excitation microscopy, Phys Rev E: Stat Nonlin Soft Matter Phys, 75: 061904 (2007).
70. Mondal, P.P. and Diaspro, A. Lateral resolution improvement in two photon excitation microscopy by aperture engineering, Opt. Comm, 281: 1855–1859 (2008).
71. Scherz, P.J., Huisken, J., Sahai-Hernandez, P. and Stainier, D.Y.R. High-speed imaging of developing heart valves reveals interplay of morphogenesis and function, Development, 135: 1179–1187 (2008).
72. Bertero, M. and Boccacci, P. "Introduction of Inverse Problems in Imaging", IOP, London, (1998).
73. Sheppard, C.J.R. and Torok, B. "An electromagnetic theory of imaging in fluorescence microscopy and imaging in polarization fluorescence microscopy", Biomimaging 5: 205 (1997).
74. Thompson, R.E., Larson, D.R. and Webb, W.W. Precise nanometer localization analysis for individual fluorescent probes, Biophys J., 82: 2775–2783 (2002).
75. Mondal, P.P., Vicidomini, G. and Diaspro, A. Image reconstruction for multi-photon fluorescence microscopy, Applied Physics Letters, 92: 103902 (2008).
76. Xu, C., Zipfel, W., Shear, J.B., Williams, R.M. and Webb, W.W. Multiphoton fluorescence excitation: New spectral windows for biological nonlinear microscopy, Proc. Nat. Acad. Scie. USA, 93: 10763–10768 (1996).
77. Alberto Diaspro Ed., Nanoscopy and Multidimensional Optical Fluorescence Microscopy, Chapman Hall/CRC, USA, (2010).
78. Wolf, E. Electromagnetic diffraction in optical systems I: An integral representation of the image field, Proc. Roy. Soc. A 253: 349 (1959).
79. Richards, B. and Wolf, E. Electromagnetic diffraction in optical systems I: Structure of the image field, Proc. Roy. Soc. A 253: 358 (1959).

Partha Pratim Mondal received his M.Sc. degree in Physics from Jawaharlal Nehru University, New Delhi, India in 2000. He earned his PhD degree in Physics from Indian Institute of Science, Bangalore, India in 2006. He is currently an Assistant Professor at the department of Instrumentation and Applied Physics, Indian Institute of Science, Bangalore, India. Before joining IISc as an Assistant Professor, he was a postdoctotal research associate at Massachusetts Institute of Technology, MA, USA; ICTP, Italy and University of Genova, Italy. He has authored more than 25 journal papers and more than 5 book chapters and many conference papers. He is a recipient of INSA Medal for Young Scientist, 2012 and DAE Young Scientist Research Award, 2011. He is currently serving as an Associate Editor for Nature Scientific Reports journal and as an Academic Editor at AIP Advances journal. His research areas focuses on, super-resolution microscopy, Bessel beam based fluorescence microscopy, Light Sheet Microscopy, Imaging Cytometry, Image Reconstruction, Multiphoton Microscopy, MESO Microscopy, PSF Engineering and Nanoscale Biological Imaging.

Shilpa Dilipkumar received her Bachelor of Engineering (B.E) degree in Instrumentation Technology from Vishweshwaraiah Technological University, Belgaum, India in 2005 and her Master of Science (M.S) degree from Electrical and Computer Engineering department, Illinois Institute of Technology, Chicago, USA in 2008. She is currently pursuing her Ph.D from Department of Instrumentation and Applied Physics, Indian Institute of Science, Bangalore, India. Her research interests include PSF engineering for super-resolution microscopy, 3D image reconstruction techniques for fluorescence microscopy and temporal resolution improvement for nanoimaging.

Kavya. M has received her B.Sc degree from Kuvempu University, Karnataka in the year 2010 and her Master degree (M.Sc) in Physics from Davanagere University in the year 2012. Now she is working as a Ph.D student in Instrumentation and Applied Physics Department in Indian Institute of Science, Bangalore, India. Her research interest includes Aperture Engineering of PSF for super resolution imaging, imaging Flow cytometry, imaging using Bessel-like beam and light sheet based Fluorescence microscopic techniques.

Raju Regmi completed his undergraduate degree in Physics from Tribhuvan University, Nepal. After completing his MSc. Physics from Bishop Heber College (Bharathidasan University), Tamilnadu, India in April, 2012 he joined NanoBioImaging Laboratory at Indian Institute of Science, Bangalore as an international research student. With broad research interest in areas of nanoscale physics and super resolution microscopy, he is currently working in the field of Imaging Flow Cytrometry Techniques and Optofluidics for his M.Sc (Engg.) degree.

Subhajit B. Purnapatra received his Bachelor of Technology (B.Tech) degree in Electronics Engineering from Indian School of Mines, Dhanbad, India, in 2010. Following his graduation, he joined the Time and Frequency Division of National Physical Laboratory, New Delhi, India, as a project assistant and contributed towards research and development of the electronic and control sub-systems for the Cesium Atomic Fountain Clock project. He is presently pursuing MSc. (Engg.) degree in the Department of Instrumentation and Applied Physics, Indian Institute of Science, Bangalore, India. He is working on, Fluorescence Microscopy and Nanoscale Biological Imaging.